TABLE OF CONTENT

Fig.S14 CD spectra of the CuS4 complex in the Vis region as a function of pH.

Fig.S15 ESI mass spectrum of the CuS5 (Cu:L = 1:1 molar ratio) in aqueous solution (pH ~ 7) along with experimental and simulated spectra of $[CuH_{-1}L]^+$ molecular ion (*m*/*z* = 1229.6 Da).

Fig.S16 LC-ESI-MS spectra of the Cu(II):S5:H_2O_2:Asc = 1:1:4:20 system at 11.3-12.1 min.

Fig.S17 Extracted ion chromatograms of the (A) Cu(II):S5:Asc = 1:1:20 and (B) Cu(II):S5:H_2O_2:Asc = 1:1:4:20 systems (blue: 584.8 ± 0.1 *m/z*, red: 592.8 ± 0.1 *m/z*, green 600.8 ± 0.1 *m/z*).

Protonation constants of Ac-ADGKAHFPRE-NH_2 (S4) and Ac-HDGKAAFPRE-NH_2 (S5) ligands

Both studied ligands behave as tetraprotic acids (H_4L) in aqueous solution. This means that they have four protonation sites that can be assigned to: two carboxyl groups (one from the side chain of the aspartic acid residue and one from the side chain of the glutamic acid residue), one imidazole moiety from the side chain of the histidyl residue, and one amino group from the lysyl residue. The formation constants (logβ) and protonation constants (log$K$) calculated from the potentiometric titration data are summarized in **Table S3**. The lowest protonation constant (log$K$ = 3.15 and 3.37 for S4 and S5 ligands, respectively) can be assigned to the carboxyl group from the side chain of the aspartyl acid residue.[1] The next protonation constant (log$K$ = 4.22 and 4.40 for S4 and S5, respectively) corresponds to the carboxyl group from the side chain of the glutamic acid residue and is consistent with other log$K$ values for this group reported in the literature.[2] In turn, log$K$ = 6.48 for S4 and 6.51 for S5 refer to the addition of a proton to the pyridine nitrogen of the imidazole ring.[3] The most basic log$K$ values (10.28 and 10.42 for S4 and S5, respectively) come from the protonation of the -NH_2 group from the side chain of the lysyl residue of the peptides.[4, 5]

Mononuclear Cu(II) complexes with S4 and S5 ligands

The presence of one histidyl residue in both sequences of the studied peptides suggests binding of one Cu(II) ion and formation of mononuclear complexes in solution. The formation and deprotonation constants calculated from potentiometric data for both Cu(II) complexes with S4 and S5 ligands are summarized in **Table S4**. The calculated logK^* values, which allow us to assess the affinity of the ligand for the Cu(II) ion, are collected in **Table 1**. Furthermore, parameters obtained using various spectroscopic methods (UV-Vis, CD, and EPR) allowed us to determine the structure of the complexes and confirm the computational models from the potentiometric experiments (**Table S5**). The stoichiometry of the formed complexes was further supported by ESI-MS, but in the gas phase.

The binding of the Cu(II) ion to S4 and S5 peptides (1:1 metal to ligand molar ratio) was studied over a wide pH range (from 2.5 to 10.5), with particular emphasis on lung pH (pH 6.7).[6] Because the lung environment is so important in our studies, the results concerning the structure of the complexes at this pH are described in the main manuscript. Here, we characterize the species formed in solution besides this pH.

Analysis of the potentiometric data revealed the formation of four (for S4) and five (for S5) mononuclear Cu(II) complexes with the general formula CuH_nL, where *n* varies from +1 to -3 (excluding 0 for **CuS4**).

The first Cu(II) complex formed in solution for S4 peptide is CuHL, which dominates at pH 5.7 and constitutes 60% of the solution (**Fig.2A**). The stoichiometry of this compound and the obtained logK^* value (-2.07) suggests that one nitrogen atom from the His residue participates in the coordination of the Cu(II) ion (**Table 1**).[7] Spectroscopic parameters such as the d-d transition at 696 nm in UV-Vis spectrum (λ_{max} calculated by Prenesti for the 1N $\{N_{im}\}$ coordination mode is 760 nm),[8, 9] the CT transition in the CD spectrum ($N_{im(\pi2)} \rightarrow$ Cu(II) at 259 nm) and EPR parameters ($A_{||}$ = 14.2 mT and $g_{||}$ = 2.332) also confirm the 1N coordination mode (**Table S5**, **Figs. S1, S2, S13A**).[10, 11] Similarly to the first complex formed with S5 peptide, the significantly lower wavelength observed for the d-d band compared to the value predicted by Prenesti may indicate the involvement of two oxygen atoms from the carboxylate groups of the Asp and Glu residues in the metal coordination sphere.[8] Above pH 5.0, another species ($CuH_{-1}L$) is formed in solution, which due to its dominance in the lung pH, has been described in detail in the main manuscript.

Further increase in pH causes deprotonation of the third amide nitrogen atom (p$K_{a(-1/-2)}$ = 8.34) and formation of the $CuH_{-2}L$ species (**Table S4**).[4] This complex constitutes ~80% of the solution at pH 9.3 (**Fig.2A**). The calculated logK^* value (-23.07) confirms the 4N $\{N_{im},3N^-\}$ coordination mode for the $CuH_{-2}L$ species and suggests that this complex is significantly more stable (about four log units) than **CuS5** with the same binding sites (**Table 1**).[12] The $CuH_{-2}L$ species also has comparable stability to **CuS2** complex (Cu(II)-Ac-WSHPQFEK-NH_2, which we studied previously) and is about one log unit less stable than **CuS1** (Cu(II)-Ac-ELDKYFKNH-NH_2) (**Table 1**).[13] The d-d band in the UV-Vis spectrum at 521 nm and shoulder at 581 nm (λ_{max} = 523 for 4N $\{N_{im}, 3N^-\}$ donor atoms predicted from the Prenesti equation)[9], CT transitions in the CD spectrum ($N_{im(\pi2)} \rightarrow$ Cu(II) at 257 nm, $N_{amid} \rightarrow$ Cu(II) at 294 nm and $N_{im(\pi1)} \rightarrow$ Cu(II) at 319 nm), as well as the EPR parameters ($A_{||}$ = 17.0 mT and $g_{||}$ = 2.228) confirm the binding of the Cu(II) ion by four nitrogen donor atoms (**Table S5**, **Figs. S1**, **S2, S13B**).[8, 14] In addition, two d-d bands at 484 and 643 nm are observed in the Vis region of the CD spectrum (**Fig.S14**).

The last species ($CuH_{-3}L$) with p$K_{a(-2/-3)}$= 10.17 calculated for the reaction $CuH_{-2}L \rightleftarrows CuH_{-3}L + H^+$ corresponds to the dissociation of the ε-amino group from the side chain of the Lys residue, which does not participate in the metal ion binding process (**Table S4**).[2] The

spectroscopic parameters for $CuH_{-3}L$, which do not change in comparison to those determined for the previous species, confirm the existence of the 4N complex (**Table S5**).

The first two species formed for the S5 ligand were characterized in the main manuscript because both predominate in the lung environment. The next species formed in aqueous solution above pH 6.0 is $CuH_{-1}L$, which dominates by more than 80% at pH 8.5 (**Fig.2B**). Since the sample precipitated at this pH but not at pH 9, we decided to determine all parameters for this species at pH 9.0 because at this pH the $CuH_{-1}L$ constitutes approximately 75% (**Fig.2B**). The stoichiometry of the complex and the $pK_{a(0/-1)}$ value of 7.49 suggest that the second amide nitrogen atom participates in the coordination of the metal ion (**Table S4**).[15] The $\log K^*$ value obtained for 3N complex with the Cu(II) ion equals -17.13 (**Table 1**). This complex is about two and a half log units less stable than the **CuS4** compound and three and two log units less stable than the **CuS1** and **CuS2** complexes (with different spike protein fragments), respectively (**Table 1**).[13] The d-d band in the UV-Vis spectrum at 601 nm (according to the Prenesti method, λ_{max} = 584 nm for the 3N $\{N_{im}, 2N^-\}$ coordination mode)[9] and the CT transitions in the CD spectrum ($N_{im(\pi 2)} \rightarrow$ Cu(II) at 256 nm and $N_{amid} \rightarrow$ Cu(II) at 314 nm)[16] prove that the Cu(II) ion is bound by one imidazole nitrogen atom and two amide donors in the $CuH_{-1}L$ species (**Table S5**, **Figs. 3C**, **S3**). Moreover, the ESI-MS spectrum of the **CuS5** complex recorded in the positive ion mode at a 1:1 metal to ligand molar ratio confirms the formation of the molecular ion $CuH_{-1}L^+$ (m/z 1229.6 Da) in the gas phase (**Fig. S15**).

Further deprotonation of the $CuH_{-1}L$ species with $pK_{a(-1/-2)}$= 9.47 calculated for the $CuH_{-1}L \rightleftarrows CuH_{-2}L + H^+$ reaction can be attributed to the dissociation of the third amide nitrogen atom from the S5 ligand and coordination of the metal ion (**Table S4**).[17] This species dominates at pH 10.3, where it constitutes ~80% of the solution. The spectroscopic parameters (d-d band in the UV-Vis spectrum at 565 nm (λ_{max} = 523 for the 4N$\{N_{im}, 3N^-\}$ coordination mode suggested by Prenesti)[9] and CT transitions in the CD spectrum ($N_{im(\pi 2)} \rightarrow$ Cu(II) at 254 nm, $N_{amid} \rightarrow$ Cu(II) at 291 nm and $N_{im(\pi 1)} \rightarrow$ Cu(II) at 334 nm) confirm the 4N$\{N_{im}, 3N^-\}$ coordination mode (**Tables 1, S5**, **Figs.3C**, **S3**).[18] The calculated $\log K^*$ value (-26.60) for $CuH_{-2}L$ species appears to be about three and a half, four and a half and four units lower than these obtained for **CuS4**, **CuS1** and **CuS2** complexes with the same binding sites, respectively (**Table 1**).[13] It may suggest that 4N complex of **CuS5** is less stable than mentioned above complexes with spike protein fragments (with the same coordination modes).

The last species, $CuH_{-3}L$, is formed above pH 9.0 with a $pK_{a(-2/-3)}$ value of 11.13 (**Table S4**, **Fig.2B**).[19] Although this value is unusually high for lysyl residue deprotonation, it may be influenced by the highly negatively charged environment of the peptide and the low

concentration. Therefore, a definitive assignment to lysyl residue deprotonation cannot be made. Spectroscopic characterization of this complex is not possible due to the overlapping of $CuH_{-3}L$ with the previous species ($CuH_{-2}L$) (**Fig.2B**).

References

1 N. E. Wezynfeld, A. Tobolska, M. Mital, U. E. Wawrzyniak, M. Z. Wiloch, D. Płonka, K. Bossak-Ahmad, W. Wróblewski and W. Bal, $A\beta_{5-x}$ Peptides: N-Terminal Truncation Yields Tunable Cu(II) Complexes, *Inorg Chem.*, 2020, **59**, 14000-14011.

2 M. Lukács, G. Szunyog, Á. Grenács, N. Lihi, C. Kállay, G. Di Natale, T. Campagna, V. Lanza, G. Tabbi, G. Pappalardo, I. Sóvágó and K. Várnagy, Copper(II) Coordination Abilities of the Tau Protein's N-Terminus Peptide Fragments: A Combined Potentiometric, Spectroscopic and Mass Spectrometric Study, *Chempluschem*, 2019, **84**, 1697-1708.

3 Z. Kastal, A. Balabán, S. Vida, C. Kállay, L. Nagy, K. Várnagy and I. Sóvágó, Copper(II), Nickel(II) and Zinc(II) Complexes of Peptide Fragments of Tau Protein, *Molecules*, 2024, **29**, 2171.

4 B. D. Balogh, B. Szakács, G. Di Natale, G. Tabbì, G. Pappalardo, I. Sóvágó and K. Várnagy, Copper (II) binding properties of an octapeptide fragment from the R3 region of tau protein: A combined potentiometric, spectroscopic and mass spectrometric study, *J Inorg Biochem.*, 2021, **217**, 111358.

5 C. A. Damante, K. Osz, Z. Nagy, G. Pappalardo, G. Grasso, G. Impellizzeri, E. Rizzarelli and I. Sóvágó, The metal loading ability of beta-amyloid N-terminus: a combined potentiometric and spectroscopic study of copper(II) complexes with beta-amyloid(1-16), its short or mutated peptide fragments, and its polyethylene glycol (PEG)-ylated analogue, *Inorg Chem.*, 2008, **47**, 9669-9683.

6 L. Gaohua, X. Miao and L. Dou, Crosstalk of physiological pH and chemical pKa under the umbrella of physiologically based pharmacokinetic modeling of drug absorption, distribution, metabolism, excretion, and toxicity, *Expert Opin Drug Metab Toxicol.*, 2021, **17**, 1103-1124.

7 M. K. Lesiów, U. K. Komarnicka, K. Stokowa-Sołtys, K. Rolka, A. Łęgowska, N. Ptaszyńska, R. Wieczorek, A. Kyzioł and M. Jeżowska-Bojczuk, Relationship between copper(ii) complexes with FomA adhesin fragments of F. nucleatum and colorectal cancer. Coordination pattern and ability to promote ROS production, *Dalton Trans.*, 2018, **47**, 5445-5458.

8 M. K. Lesiów, P. Pietrzyk, A. Bieńko and T. Kowalik-Jankowska, Stability of Cu(ii) complexes with FomA protein fragments containing two His residues in the peptide chain, *Metallomics*, 2019, **11**, 1518-1531. Erratum in: *Metallomics*, 2020. **12**, 2199.

9 E. Prenesti, P. G. Daniele, M. Prencipe and G. Ostacoli, Spectrum-structure correlation for visible absorption spectra of copper(II) complexes in aqueous solution, *Polyhedron*, 1999, **18**, 3233-3241.
10 I. Naletova, G. I. Grasso, C. Satriano, A. Travaglia, D. La Mendola, G. Arena and E. Rizzarelli, Copper complexes of synthetic peptides mimicking neurotrophin-3 enhance neurite outgrowth and CREB phosphorylation, *Metallomics*, 2019, **11**, 1567-1578.
11 G. Di Natale, G. Grasso, G. Impellizzeri, D. La Mendola, G. Micera, N. Mihala, Z. Nagy, K. Osz, G. Pappalardo, V. Rigó, E. Rizzarelli, D. Sanna and I. Sóvágó, Copper(II) interaction with unstructured prion domain outside the octarepeat region: speciation, stability, and binding details of copper(II) complexes with PrP106-126 peptides, *Inorg Chem.*, 2005, **44**, 7214-7225.
12 M. Kuczer, M. Pietruszka and T. Kowalik-Jankowska, Copper(II) complex formation processes of alloferon I with point mutation H1K; combined spectroscopic and potentiometric studies, *J Inorg Biochem.*, 2012, **111**, 40-49.
13 M. K. Lesiów, M. Witwicki, N. K. Tan, M. E. Graziotto and E. J. New, Unravelling the Mystery of COVID-19 Pathogenesis: Spike Protein and Cu Can Synergize to Trigger ROS Production, *Chemistry*, 2023, **29**, e202301530.
14 M. K. Lesiów, B. Kwiatkowski, P. Pietrzyk, A. Kyzioł, K. Rolka and U. K. Komarnicka, *Fusobacterium nucleatum*'s Copper-FomA Proteins: Driving Cancer Forward, *Inorg Chem.*, 2025, **64**, 15502-15517.
15 A. Kadej, M. Kuczer and T. Kowalik-Jankowska, Copper(II) complexes of terminally free alloferon mutants containing two histidyl binding sites inside peptide chain structure and stability, *Dalton Trans.*, 2015, **44**, 20659-20674.
16 T. Kowalik-Jankowska, E. Jankowska, Z. Szewczuk and F. Kasprzykowski, Coordination abilities of neurokinin A and its derivative and products of metal-catalyzed oxidation, *J Inorg Biochem.*, 2010, **104**, 831-842.
17 E. Székely, M. Molnár, N. Lihi and K. Várnagy, Characterization of Copper(II) and Zinc(II) Complexes of Peptides Mimicking the CuZnSOD Enzyme, *Molecules*, 2024, **29**, 795.
18 T. Kowalik-Jankowska, Ł. Biega, M. Kuczer and D. Konopińska, Mononuclear copper(II) complexes of alloferons 1 and 2: a combined potentiometric and spectroscopic studies, *J Inorg Biochem.*, 2009, **103**, 135-142.
19 M. Błaszak, E. Jankowska and T. Kowalik-Jankowska, Acid-base properties of the (1-4,18-36) fragments of neuropeptide K and their mono- and polynuclear copper(II) complexes products of metal-catalyzed oxidation, *Inorg Chem.*, 2013, **52**, 130-143.

Table S1 The formation (logβ) and protonation constants (log$K$) for **S4** and **S5** peptides (used in experiments performed with transition metal ions besides Cu(II) ions; I = 0.2 M KCl, T = 298 K).

Species	**S4**	**S5**
	logβ*	
HL	10.12(3)	10.04(5)
H_2L	16.68(1)	16.46(7)
H_3L	20.99(1)	20.71(9)
H_4L	24.25(1)	23.95(12)
	log$K$	
NH_2 (Lys)	10.12	10.04
His	6.56	6.42
COO^- (Glu)	4.31	4.25
COO^- (Asp)	3.26	3.24

*Formation constants (logβ) and protonation constants (log$K$) for ligand are expressed by the equations: $\beta(H_nL)=[H_nL]/[L][H^+]^n$ and $\log K=\log\beta(H_nL)-\log\beta(H_{n-1}L)$, respectively. Standard deviations (3σ values) on the last digit of formation and protonation constants are given in parentheses. Charges are omitted for clarity.

Table S2 The formation (logβ) and deprotonation constants (pK_a) for **S4** and **S5** peptides with appropriate transition metal ions (I = 0.2 M KCl, T = 298 K).

Species	**S4**						**S5**					
	Zn(II)	**Mn(II)**	**Fe(III)**	**Fe(II)**	**Ni(II)**	**Co(II)**	**Zn(II)**	**Mn(II)**	**Fe(III)**	**Fe(II)**	**Ni(II)**	**Co(II)**
logβ^*												
MH_2L	-	-	-	19.75(11)	-	-	-	-	-	19.22(10)	-	-
MHL	-	-	15.85(13)	15.14(7)	13.71(6)	13.95(9)	-	-	15.59(12)	14.36(6)	-	13.23(11)
ML	-	-	-	8.56(8)	5.47(6)	5.36(8)	-	-	-	7.24(10)	-	4.37(14)
$MH_{-1}L$	-3.46(7)	-5.73(28)	-	-	-	-	-3.55(8)	-5.76(11)	-	-	-	-4.48(5)
$MH_{-2}L$	-14.27(11)	-	-	-	-11.58(4)	-	-14.57(12)	-	-	-	-13.93(10)	-
$MH_{-3}L$	-	-	-	-	-21.57(6)	-	-	-	-	-	-	-
pK_a^*												
p$K_{(2/1)}$	-	-	-	4.61	-	-	-	-	-	4.86	-	-
p$K_{(1/0)}$	-	-	-	6.58	8.24	8.59	-	-	-	7.12	-	8.86

p$K_{(0/-1)}$	-	-	-	-	-	-	-	-	-	-	-	8.85
p$K_{(-1/-2)}$	10.81	-	-	-	-	-	11.02	-	-	-	-	-
p$K_{(-2/-3)}$	-	-	-	-	9.99	-	-	-	-	-	-	-

*Formation constants (logβ) and deprotonation constants (pK_a) for the ML complex are expressed by the following equations: $\beta(MH_nL)=[MH_nL]/[M][L][H^+]^n$ and $pK_a=\log\beta(MH_nL)-\log\beta(MH_{n-1}L)$, respectively. Standard deviations (3σ values) on the last digit of formation and protonation constants are given in parentheses. Charges are omitted for clarity.

Table S3 The formation (logβ) and protonation constants (log$K$) for **S4** and **S5** peptides (used for experiment with Cu(II) ions; I = 0.1 M KNO_3, T = 298 K).

Species	**S4**	**S5**
	logβ^*	
HL	10.28(1)	10.42(1)
H_2L	16.76(1)	16.94(1)
H_3L	20.98(1)	21.33(1)
H_4L	24.12(1)	24.71(1)
	log$K$	
NH_2 (Lys)	10.28	10.42
His	6.48	6.51
COO^- (Glu)	4.22	4.40
COO^- (Asp)	3.15	3.37

*Formation constants (logβ) and protonation constants (log$K$) for ligand are expressed by the equations: $\beta(H_nL)=[H_nL]/[L][H^+]^n$ and $\log K=\log\beta(H_nL)-\log\beta(H_{n-1}L)$, respectively. Standard deviations (3σ values) on the last digit of formation and protonation constants are given in parentheses. Charges are omitted for clarity.

Table S4 Formation constants (logβ) and calculated deprotonation constants (pK_a) for mononuclear Cu(II) complexes of **CuS4** and **CuS5** (I = 0.1 M KNO_3, T = 298 K).

Species	**CuS4**	**CuS5**
	logβ^*	
CuHL	14.69(1)	14.43(1)
CuL	-	7.30(1)
$CuH_{-1}L$	2.03(1)	-0.19(1)
$CuH_{-2}L$	-6.31(1)	-9.66(1)
$CuH_{-3}L$	-16.48(1)	-20.79(2)
	pK_a^*	
p$K_{(1/0)}$	-	7.14
p$K_{(0/-1)}$	-	7.49
p$K_{(-1/-2)}$	8.34	9.47
p$K_{(-2/-3)}$	10.17	11.13

*Formation constants (logβ) and deprotonation constants (pK_a) for the CuL complex are expressed by the following equations: $\beta(CuH_nL)=[CuH_nL]/[Cu][L][H^+]^n$ and $pK_a=\log\beta(CuH_nL)-\log\beta(CuH_{n-1}L)$, respectively. Standard deviations (3σ values) on the last digit of formation and protonation constants are given in parentheses. Charges are omitted for clarity.

Table S5 Spectroscopic parameters for the mononuclear complexes of **CuS4** and **CuS5**.

Species	pH	UV-Vis		CD		EPR					
		λ [nm]	ε [$M^{-1}cm^{-1}$]	λ [nm]	$\Delta\varepsilon$ [$M^{-1}cm^{-1}$]	$g_{\|\|}$ (g_{zz})	$g_{\perp}$ (g_{xx})	$g_{\perp}$ (g_{yy})	$^{Cu}A_{\|\|}$ [mT]	$^{Cu}A_{\perp}$ [mT]	$^{N}A_{\perp}$ [mT]
CuS4 1:1											
CuHL **1N {N_{im}}**	5.9	696[a]	26	259[b]	0.31	2.332	2.065	2.069	14.2	unresolved	unresolved
$CuH_{-1}L$ **3N {N_{im}, $2N^{-}$}**	7.2	597[a]	48	253[b] 336[c,d] 536[a] 691[a]	4.78 -0.77 0.35 0.10	2.224	2.049	2.058	17.3	unresolved	unresolved
$CuH_{-2}L$ **4N {N_{im}, $3N^{-}$}**	9.3	521[a] 581[a,sh]	71 65	257[b] 294[c] 319[d] 484[a] 643[a]	4.22 -0.14 0.42 -0.61 0.42	2.228	2.049	2.051	17.0	unresolved	unresolved
$CuH_{-3}L$ **4 N {N_{im}, 3 N^{-}}**	10.5	516[a] 581[a,sh]	79 68	259[b] 293[c] 320[d] 485[a] 643[a]	4.03 -0.22 0.67 -0.78 0.52	2.228	2.049	2.051	17.0	unresolved	unresolved
CuS5 1:1											
CuHL **1N {N_{im}}**	6.4	693[a]	33	-	-	-	-	-	-	-	-
$CuH_{-1}L$ **3N {N_{im}, $2N^{-}$}**	9.0	601[a]	70	256[b] 314[c] 590[a] 530[sh]	1.22 -0.28 -0.17 -0.15	-	-	-	-	-	-
$CuH_{-2}L$ **4N {N_{im}, $3N^{-}$}**	10.3	565[a]	87	254[b] 291[c]	1.77 -0.32	-	-	-	-	-	-

				334[d] 511[a]	-0.18 -0.42					

[a]*d-d* transition; sh-shoulder; [b]$N_{Im}(\pi_2)\rightarrow$Cu(II) charge transfer transition; [c]$N^{-}_{(amid)}\rightarrow$Cu(II) charge transfer transition; [d]$N_{Im}(\pi_1)\rightarrow$Cu(II) charge transfer transition.

Table S6 Summary of pseudo-first order rate constants k [min^{-1}] of R6G degradation for the studied compounds in the presence of Asc (k was calculated for the first five minutes of reaction).

Studied system + Asc	**Rate constant (k) [min^{-1}]**
R6G+Cu(II)	$2.10(2)\times10^{-2}\pm1.04\times10^{-4}$
R6G+S4	$4.88(9)\times10^{-3}\pm3.57\times10^{-5}$
R6G+S5	$5.60(9)\times10^{-3}\pm5.31\times10^{-5}$
R6G+CuS4	$1.40(2)\times10^{-2}\pm2.33\times10^{-4}$
R6G+CuS5	$1.60(3)\times10^{-2}\pm1.14\times10^{-4}$

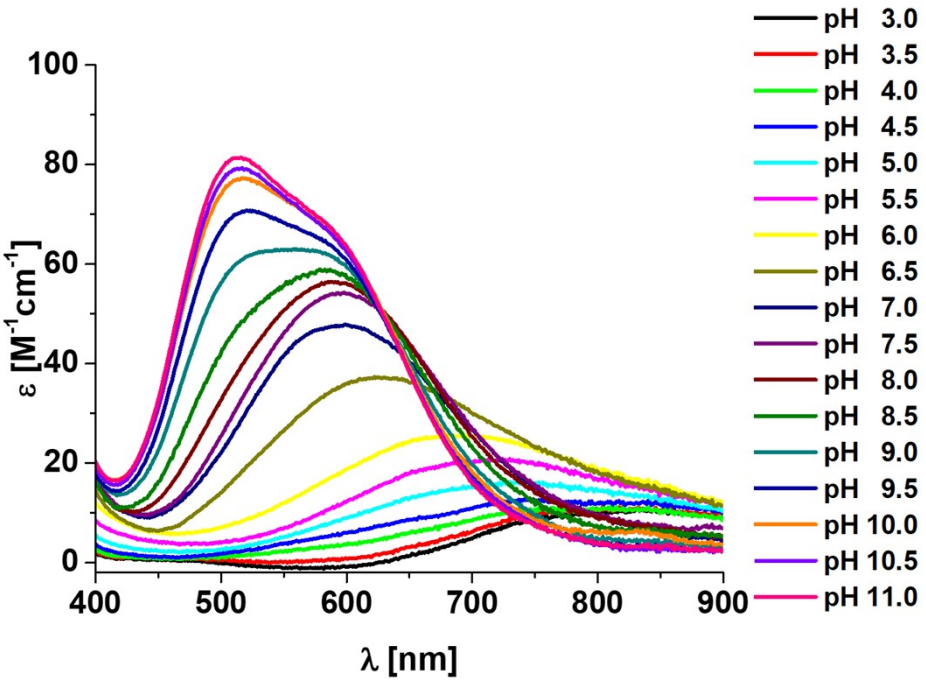

Fig.S1 Electronic absorption spectra of the **CuS4** complex as a function of pH (Cu:L = 1:1, [Cu(II)] = 0.001 M).

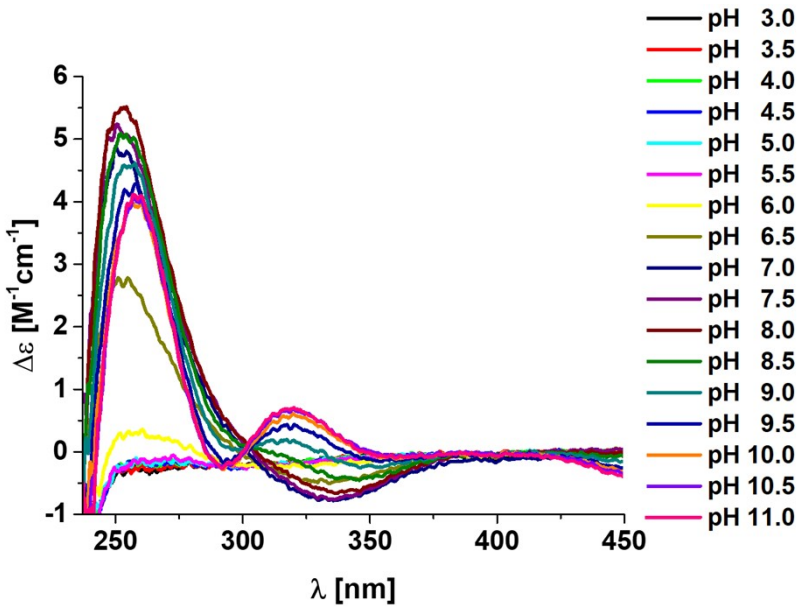

Fig.S2 CD spectra of the **CuS4** complex in the UV region as a function of pH (Cu:L = 1:1, [Cu(II)] = 0.001 M).

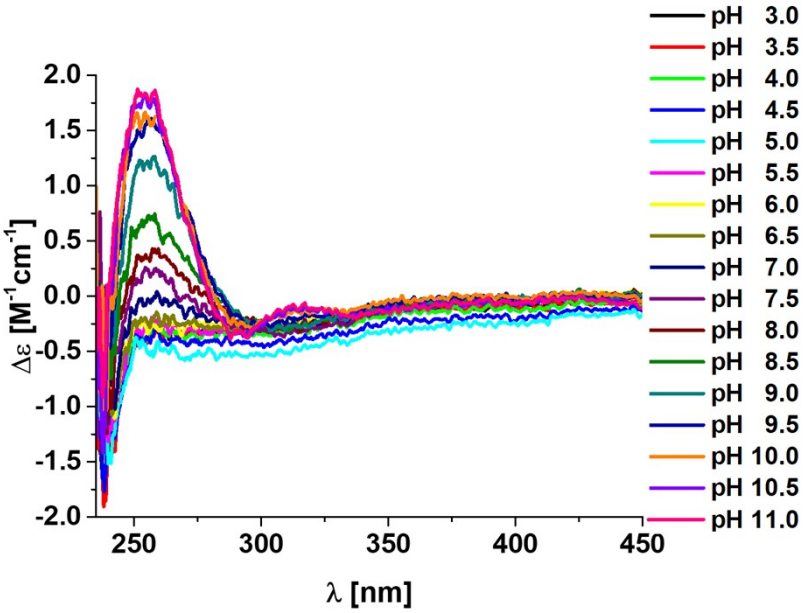

Fig.S3 CD spectra of the **CuS5** complex in the UV region as a function of pH (Cu:L = 1:1, [Cu(II)] = 0.001 M).

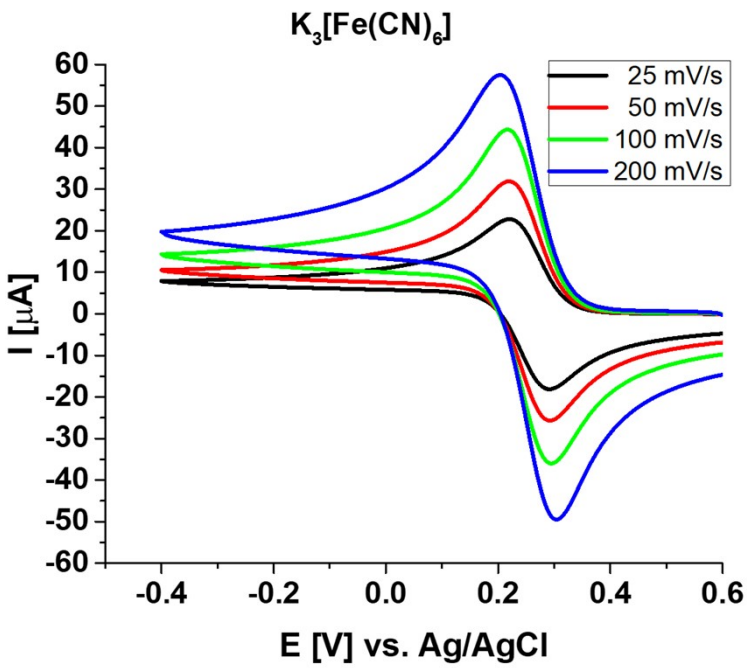

Fig.S4 Cyclic voltammetric profiles of 6 mM $K_3[Fe(CN)_6]$ with KNO_3 (0.2 M) as a supporting electrolyte in aqueous solution in different scan rates.

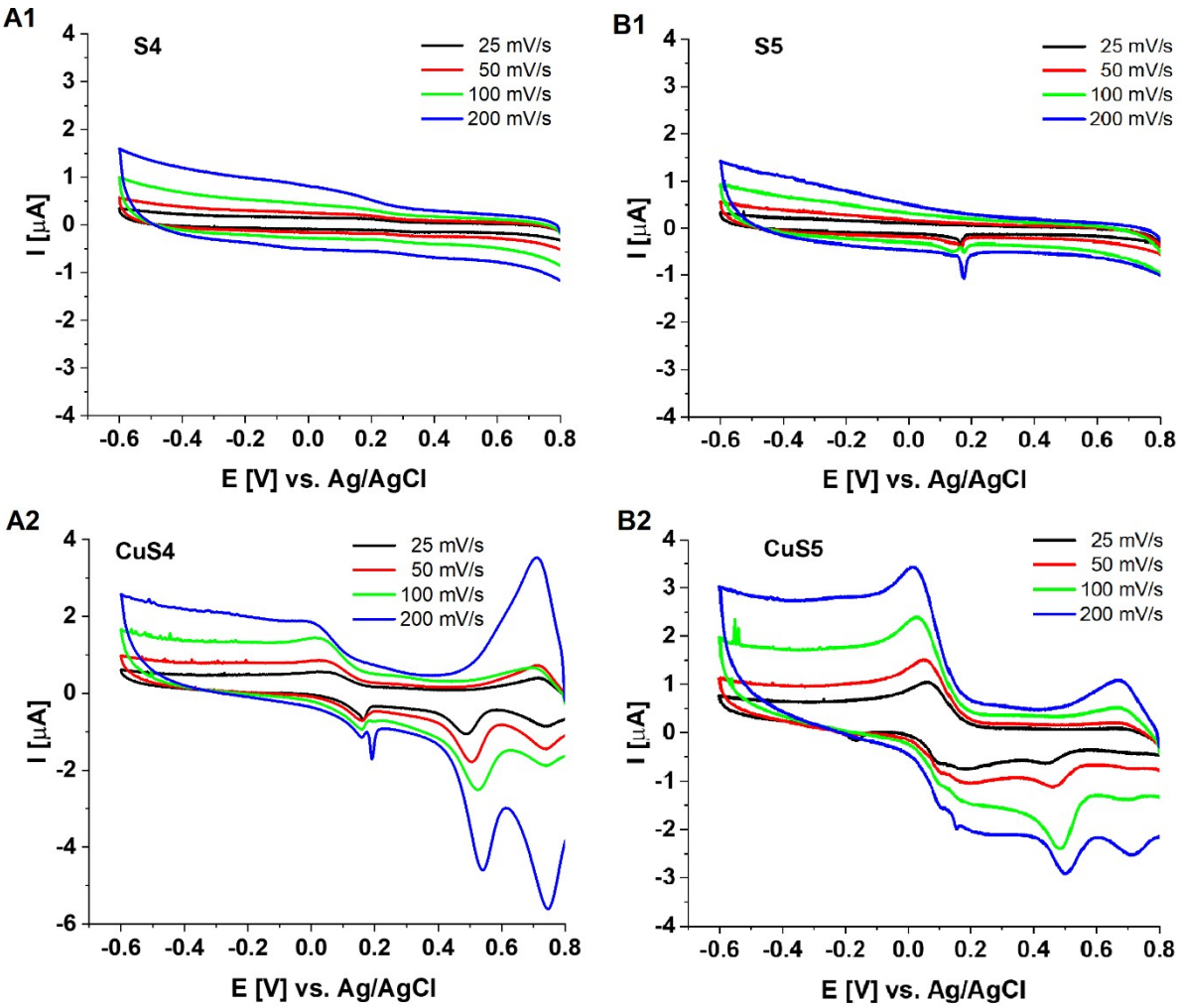

Fig.S5 Cyclic voltammetric profiles of (A1) 1 mM S4; (A2) 1 mM CuS4; (B1) 1 mM S5; and (B2) 1 mM CuS5. CV of the compounds was performed with KNO_3 (0.2 M) as a supporting electrolyte in aqueous solution at pH 6.7 and T = 298 K.

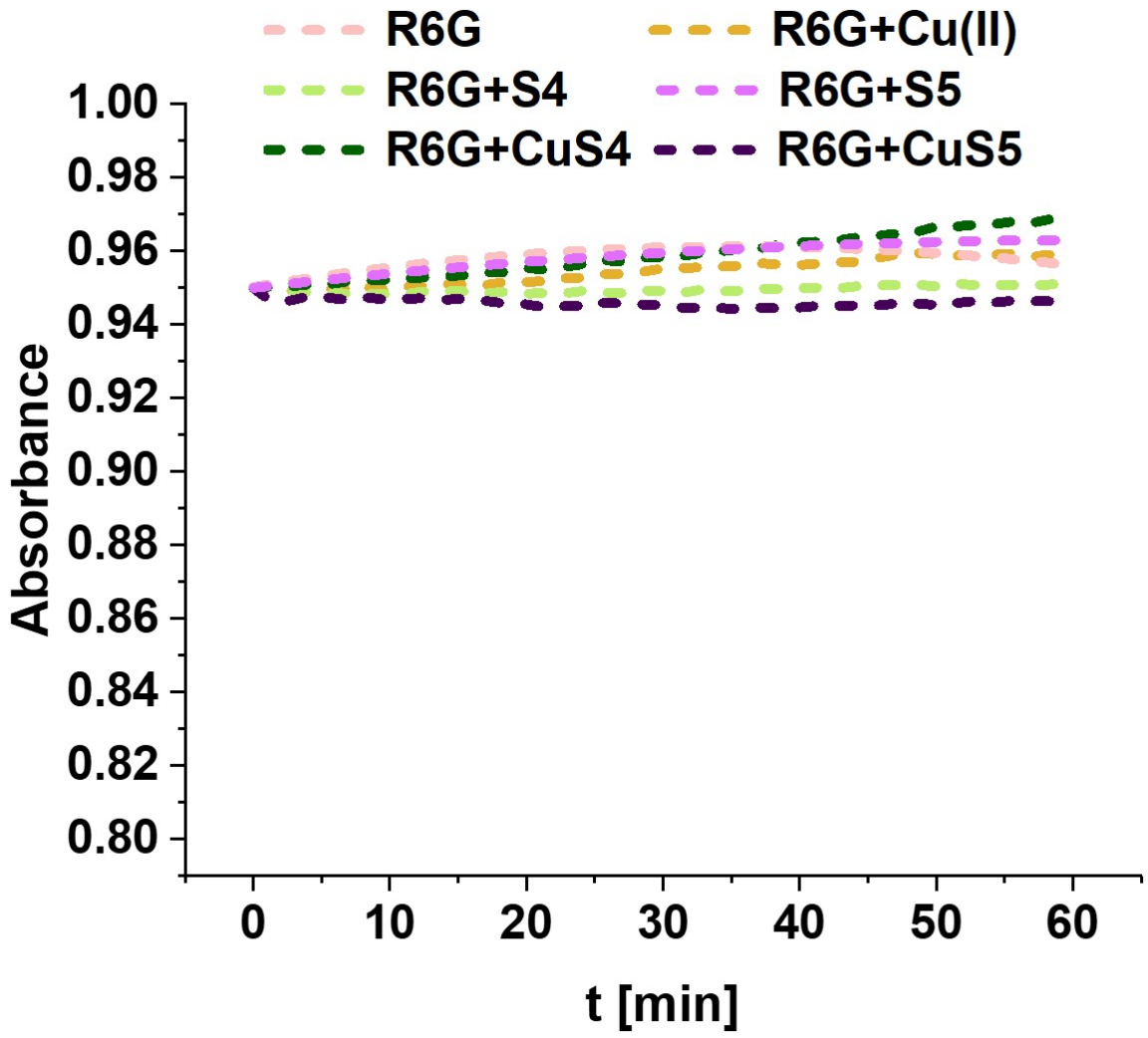

Fig.S6 The experimental kinetic curves of R6G with different compounds without H_2O_2.

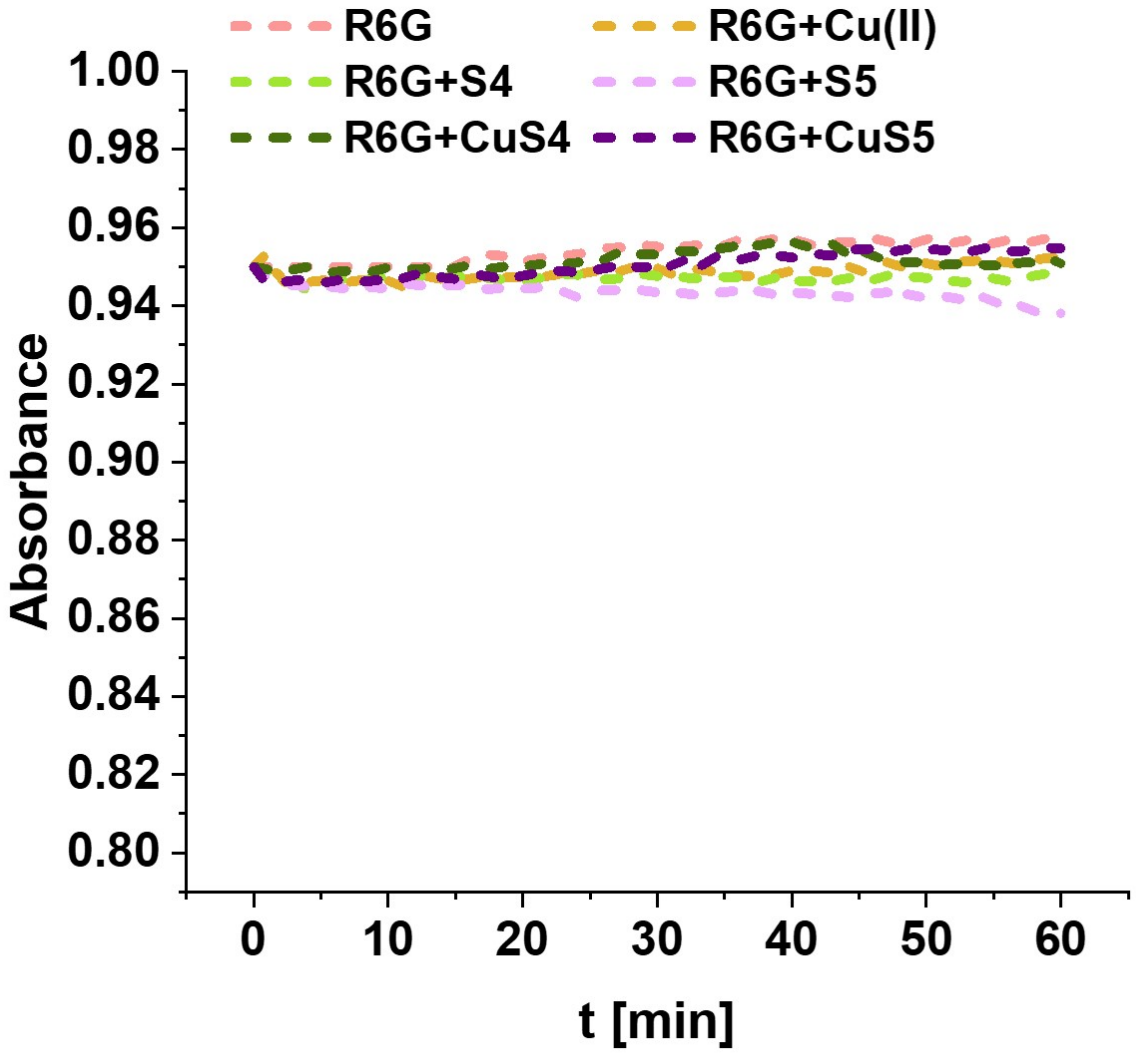

Fig.S7 The experimental kinetic curves of R6G with different compounds without Asc.

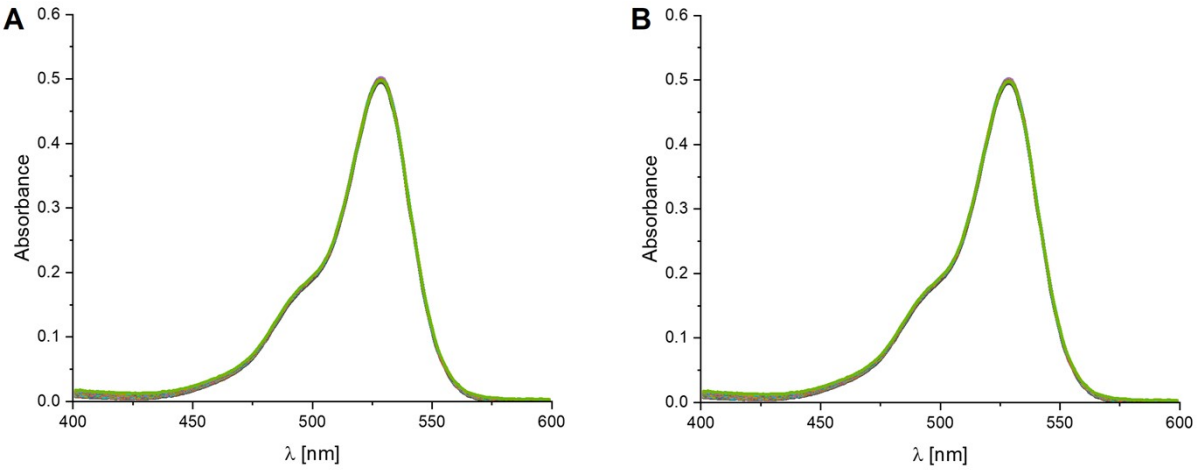

Fig.S8 Absorption spectra of R6G solutions with addition of DMSO, recorded for: A) CuS4 and B) CuS5 complex in the presence of H_2O_2.

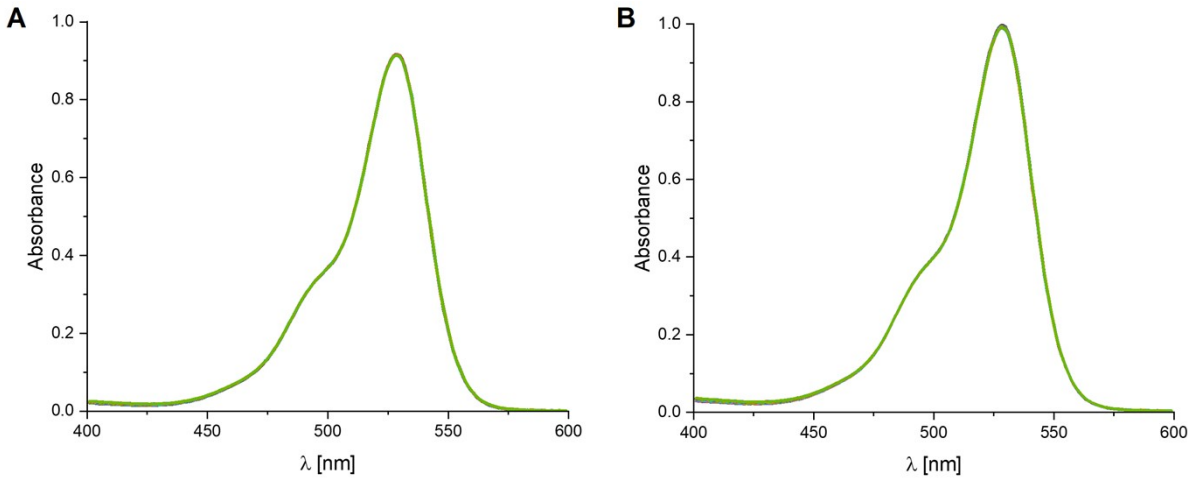

Fig.S9 Absorption spectra of R6G solutions with addition of DMSO, recorded for: A) CuS4 and B) CuS5 complex in the presence of Asc.

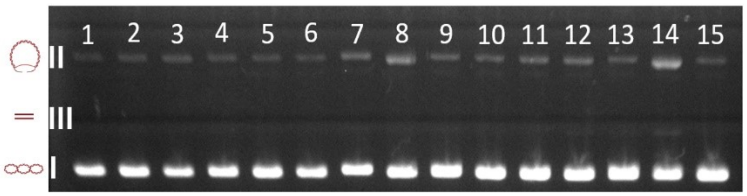

Fig.S10 Effect of **S4** and **S5** ligands (C=50 μM) with H_2O_2 (C=50 μM) at pH 6.7 on plasmid DNA (pBR322). Lanes: **1:** plasmid; **2:** plasmid+**S4**; **3:** plasmid+**S4**+H_2O_2; **4:** plasmid+**S4**+H_2O_2+DMSO; **5:** plasmid+**S4**+H_2O_2+NaN_3; **6:** plasmid+**S4**+H_2O_2+KI; **7:** plasmid+**S5**; **8:** plasmid+**S5**+H_2O_2; **9:** plasmid+**S5**+H_2O_2+DMSO; **10:** plasmid+**S5**+H_2O_2+NaN_3; **11:** plasmid+ **S5**+ H_2O_2+KI; **12:** plasmid+H_2O_2; **13:** plasmid+H_2O_2+DMSO; **14:** plasmid+H_2O_2+NaN_3; **15:** plasmid+H_2O_2+KI.

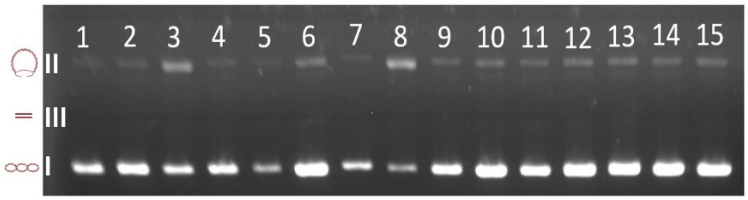

Fig.S11 Effect of **S4** and **S5** ligands (C=50 μM) with Asc (C=50 μM) at pH 6.7 on plasmid DNA (pBR322). Lanes: **1:** plasmid; **2:** plasmid+**S4**; **3:** plasmid+**S4**+Asc; **4:** plasmid+**S4**+Asc +DMSO; **5:** plasmid+**S4**+Asc+NaN_3; **6:** plasmid+**S4**+Asc+KI; **7:** plasmid+**S5**; **8:** plasmid+**S5**+Asc; **9:** plasmid+**S5**+Asc+DMSO; **10:** plasmid+**S5**+Asc+NaN_3; **11:** plasmid+ **S5**+Asc+KI; **12:** plasmid+Asc; **13:** plasmid+Asc+DMSO; **14:** plasmid+Asc+NaN_3; **15:** plasmid+Asc+KI.

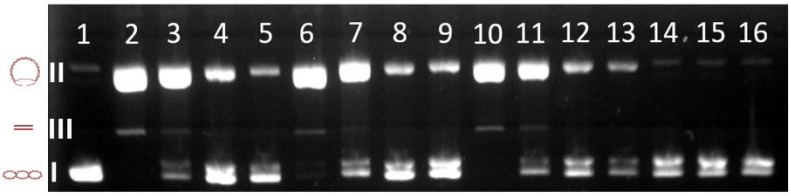

Fig.S12 Effect of uncomplexed Cu(II) ions and **CuS4** and **CuS5** complexes (C=50 μM) at pH 6.7 on plasmid DNA (pBR322). Lanes: **1:** plasmid; **2:** plasmid+Cu(II); **3:** plasmid+Cu(II)+DMSO; **4:** plasmid+Cu(II)+NaN_3; **5:** plasmid+Cu(II)+KI; **6:** plasmid+**CuS4**; **7:** plasmid+**CuS4**+DMSO; **8:** plasmid+**CuS4**+NaN_3; **9:** plasmid+**CuS4**+KI; **10:** plasmid+**CuS5**; **11:** plasmid+**CuS5**+DMSO; **12:** plasmid+**CuS5**+NaN_3; **13:** plasmid+**CuS5**+KI; **14:** plasmid+DMSO; **15:** plasmid+NaN_3; 16: plasmid+KI.

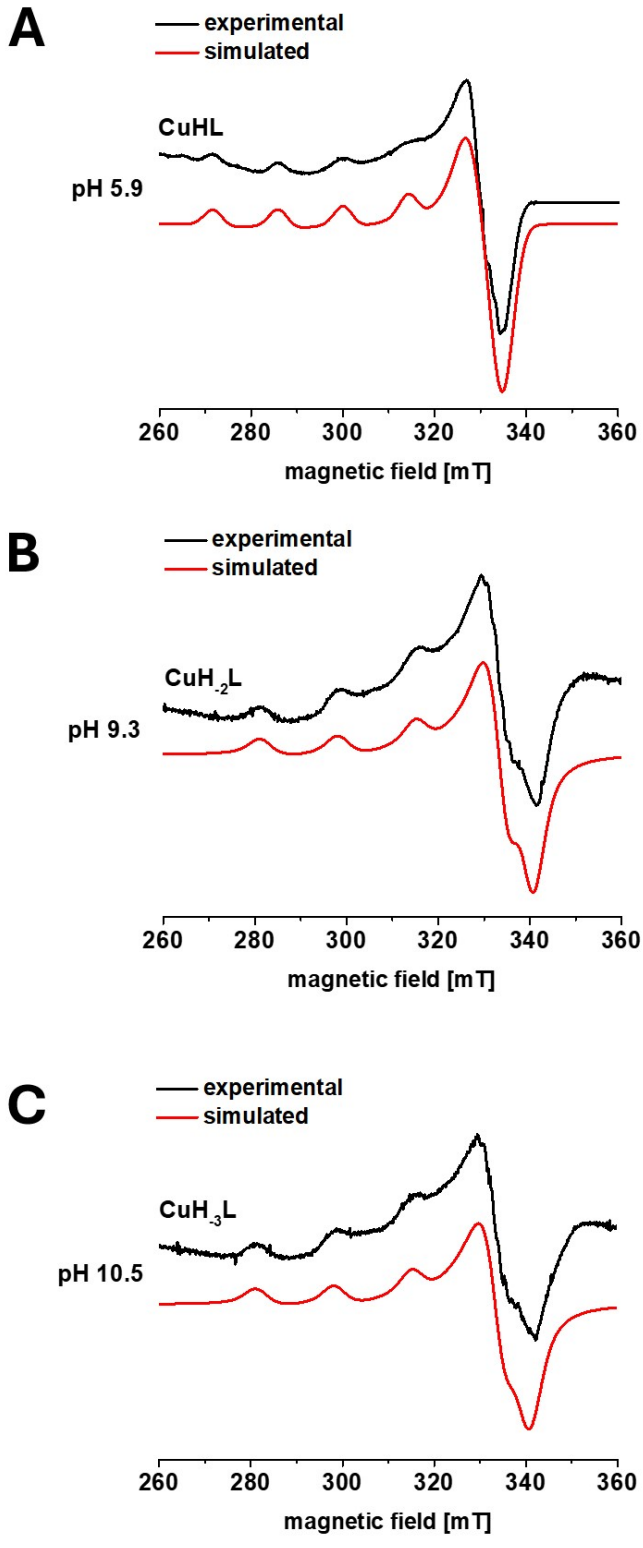

Fig.S13 EPR spectra recorded for frozen (77 K) solutions of **CuS4** complex at various pH (Cu:L =1:1, [Cu(II)] = 0.001 M).

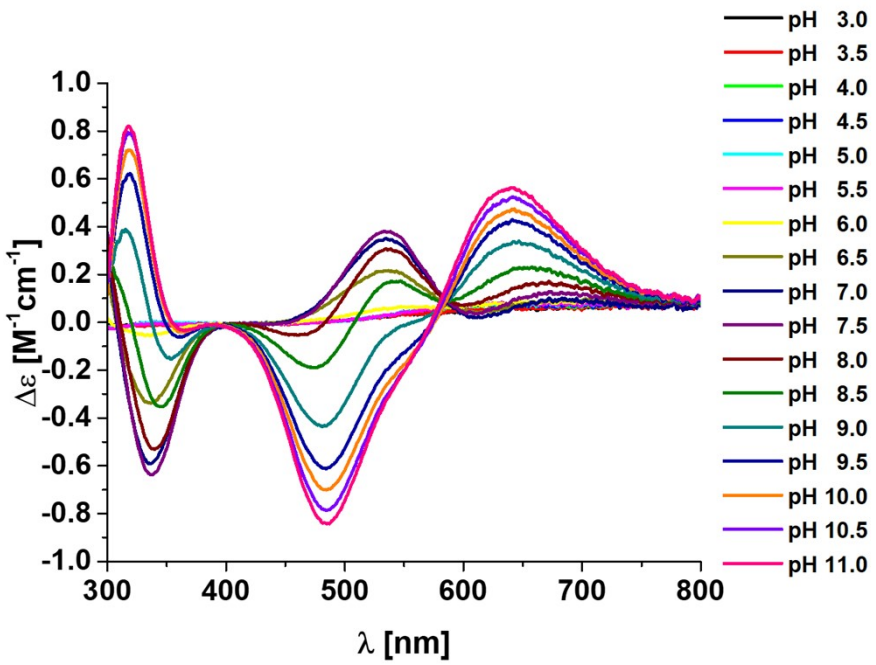

Fig.S14 CD spectra of the **CuS4** complex in the Vis region as a function of pH (Cu:L = 1:1, [Cu(II)] = 0.001 M).

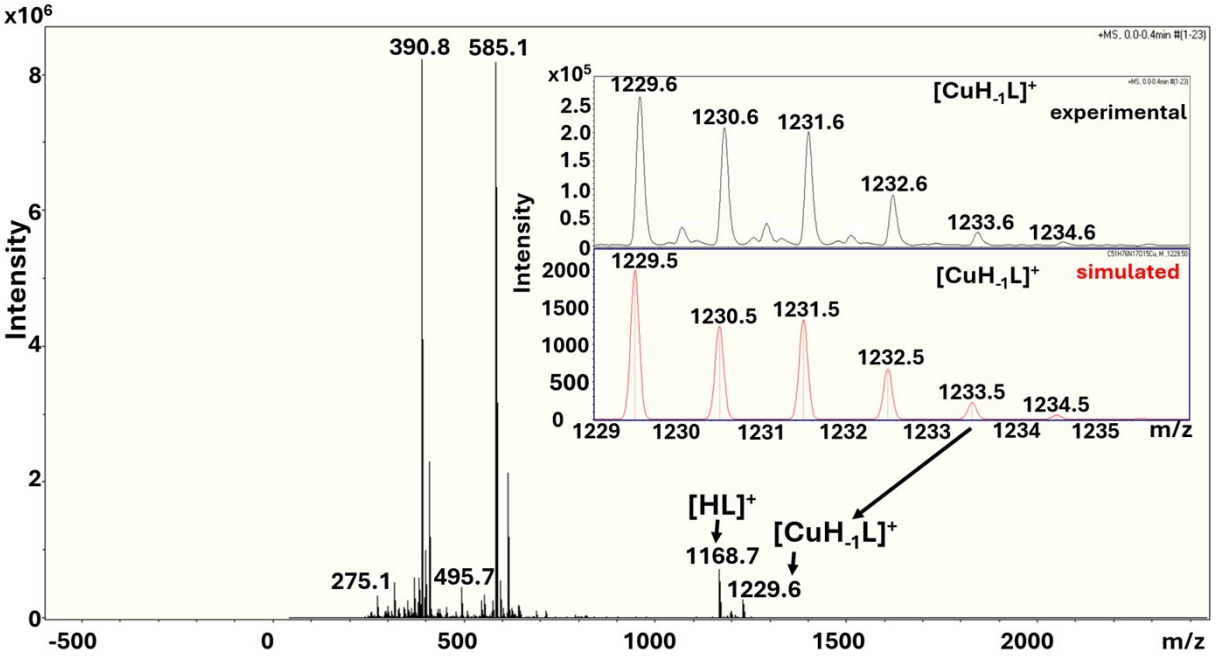

Fig.S15 ESI mass spectrum of the **CuS5** (Cu:L = 1:1 molar ratio) in aqueous solution (pH ~ 7) along with experimental and simulated spectra of $[CuH_{-1}L]^+$ molecular ion (*m*/*z* = 1229.6 Da).

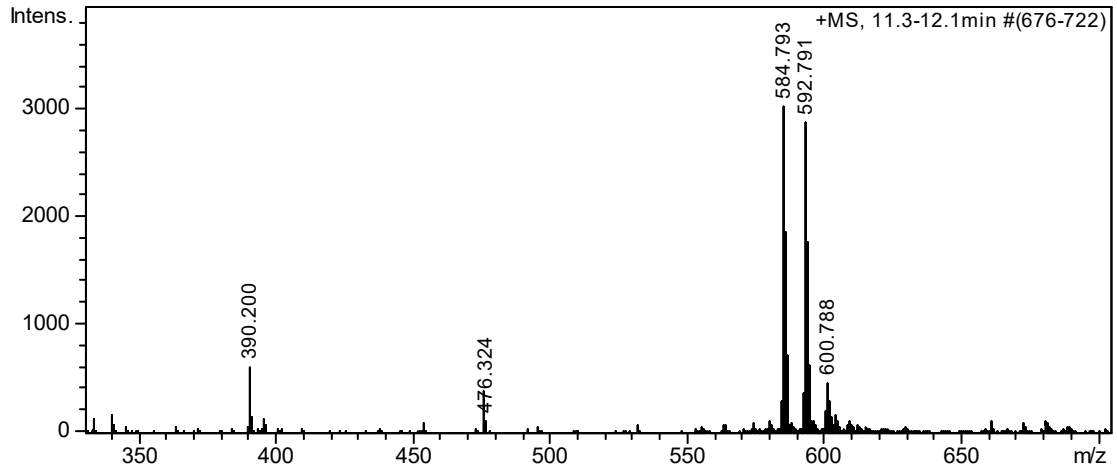

Fig. S16 LC-ESI-MS spectra of the Cu(II):S5:H_2O_2:Asc = 1:1:4:20 system at 11.3-12.1 min.

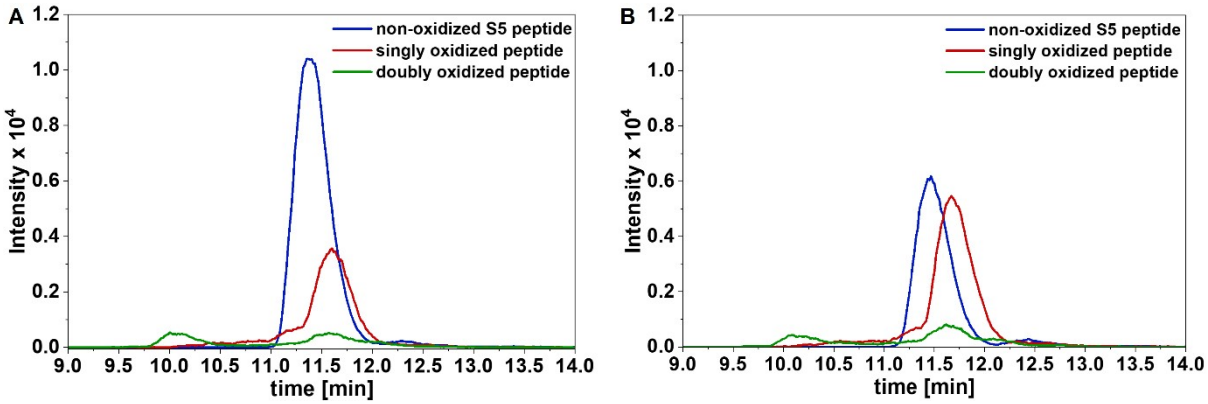

Fig. S17 Extracted ion chromatograms of the (A) Cu(II):S5:Asc = 1:1:20 and (B) Cu(II):S5:H_2O_2:Asc = 1:1:4:20 systems (blue: 584.8 ± 0.1 *m/z*, red: 592.8 ± 0.1 *m/z*, green 600.8 ± 0.1 *m/z*).